Interdisciplinary Information Sciences Vol. 22, No. 2 (2016) 215–227

ISSN 1340-9050 print/1347-6157 online
DOI 10.4036/iis.2016.A.04

Operating Conditions for the Hemodialysis Treatment Based on the Volume Averaging Theory

Yoshihiko SANO*

Department of Mechanical Engineering, Shizuoka University, 3-5-1 Johoku, Naka-ku, Hamamatsu 432-8561, Japan

The effect of operating conditions on the clearance of a countercurrent hollow fiber dialyzer has been investigated by utilizing the membrane transport model based on the volume averaging theory. The three-dimensional numerical method for describing the mass transport phenomena within a hollow fiber membrane dialyzer has been proposed to estimate performances under the several volume flow rates for blood and dialysate phases. Clearances obtained from the present numerical simulation are compared against available set of experimental data to elucidate the validity of the present three-dimensional numerical method. A series of calculations reveal the effect of the volume flow rate for blood and dialysate phases on urea clearance under the several total ultrafiltration rates. Moreover, the removal efficiency, which is the ratio of the mass flow rate of urea removed from the blood phase within a dialyzer to that at the blood phase inlet, is introduced in order to estimate an appropriate volume flow rate for blood and dialysate phases in the hemodialysis treatment. The present study clearly indicates that the present numerical method is quite useful for determining the best clinical protocol of the hemodialysis treatment and developing new dialysis systems such as home hemodialysis, nocturnal dialysis and even wearable artificial kidney.

KEYWORDS: hollow fiber dialyzer system, numerical simulation, volume averaging theory, operating condition

1. Introduction

Hollow fiber dialyzers are widely used in the therapy of hemodialysis, which is a method for removing waste products such as creatinine and urea, as well as free water from the blood when the kidneys are in renal failure. These dialyzers are utilized a bundle of hollow fibers of the ultrafiltration membrane to remove metabolic end products from the human body. Usually, patients are required to receive 3 times hemodialysis treatment per week, which it takes 3–4 hours per one treatment in Japan. In this situation, the home hemodialysis and the nocturnal dialysis have been focused to improve the quality of life for patients undergoing the hemodialysis treatment. Moreover, Davenport *et al.* [1] and Gura *et al.* [2] proposed the wearable artificial kidney downsizing the dialysis system, which is a belt type dialyzer wrapped around patients waist. However, these treatments under investigation in clinical trials have been developed based on the doctor's experience.

On the other hand, several researchers have investigated to evaluate mass transport processes through membranes within dialyzers. A number of analytical and numerical models based on the Kedem-Katchalsky model, in which estimates the volume and solute flows of nonelectrolyte solutions across membranes, have been reported in the literature [3–13]. However, in most of previous investigations, the axial concentration distribution within the dialyzer has been neglected despite three-dimensional structures. Moreover, some numerical attempts (Shirazian, *et al.* [14]; Wang *et al.* [15]; Kumar and Upadhyay [16]) appear to be difficult to elucidate the details of flow and concentration within the dialyzer containing thousands of hollow fiber membranes. Under these situations, Sano and Nakayama [17] proposed a membrane transport model based on the volume averaging theory for the analysis of hollow fiber hemodialysis systems. The concept of local volume-averaging theory, namely, VAT, widely used in the study of porous media (Cheng [18], Quintard and Whitaker [19], Nakayama [20], Vafai and Tien [21], Nakayama and Kuwahara [22], Yang and Nakayama [23]) is quite useful under these situations, in which thousands of small-scale elements exist in a large space. Subsequently, Sano *et al.* [24] provided three-dimensional numerical computations for revealing the mass transport phenomena within the three individual phases, namely the blood (lumen), the dialysate (shell) and the membrane phases in the countercurrent hollow fiber dialyzer. They confirmed the validity of their numerical simulation for creatinine and vitamin B12 by comparing clearances calculated from their simulation method and experimental data.

In this paper, we shall prove that the volume averaging theory itself is capable of describing such complex three-dimensional flow and concentration fields within hollow fiber membrane dialyzers. A rigorous mathematical

Received April 12, 2016; Accepted June 24, 2016; J-STAGE Advance published November 28, 2016
*Corresponding author. E-mail: sano.yoshihiko@shizuoka.ac.jp

development based on the volume-averaging theory is presented to obtain a complete set of the three-dimensional volume-averaged governing equations for hollow fiber membrane dialyzers. Subsequently, the effect of operating conditions on urea clearance within a dialyzer FDW-10 produced by Nikkiso has been investigated by three-dimensional numerical computations. A series of calculations have been conducted to evaluate the effect of both volume flow rates for dialysis and blood phases on urea clearance under the several total ultrafiltration rates. Moreover, new indices for the hemodialysis treatment are introduced in terms of the mass transport phenomena within dialyzers. This present numerical method is quite useful for determining the best clinical protocol of the hemodialysis treatment and developing new dialysis systems such as home hemodialysis, nocturnal dialysis and even wearable artificial kidney.

2. Volume Averaging Theory for Hollow Fiber Membrane Dialyzers

The volume averaging theory [17–23] is introduced to derive a complete set of the volume-averaged governing equations for the case of hollow fiber membrane dialyzer systems. At first, we shall consider the concept of the volume averaging theory in this chapter. The concept of the local volume-averaging theory are widely used in the study of porous media under these situations, in which thousands of small-scale elements exist in a large space. Now, we consider a local control volume V in a porous medium filled with substances, as shown in Fig. 1. Under this condition, the volume average of a certain variable ϕ is defined as

$$\langle \phi \rangle = \frac{1}{V} \int_{V_f} \phi dV \tag{1}$$

On the other hand, another average, namely, the intrinsic average, is given by

$$\langle \phi \rangle^f = \frac{1}{V_f} \int_{V_f} \phi dV \tag{2}$$

where length scale $V^{1/3}$ should be much greater than the microscopic matrix characteristic length (say the size of the hollow fiber), at the same time, length scale $V^{1/3}$ should be much smaller than the macroscopic characteristic length ${V_c}^{1/3}$, namely, the size of dialyzer [17, 19]. V_f is the volume space which the fluid (either blood or dialysate) occupies. Two averages are related as

$$\langle \phi \rangle = \varepsilon_f \langle \phi \rangle^f \tag{3}$$

where $\varepsilon_f = V_f/V$ is the local volume fraction of the fluid space. A variable is decomposed into its intrinsic average and the spatial deviation, like the Reynolds decomposition.

$$\phi = \langle \phi \rangle^f + \tilde{\phi} \tag{4}$$

Naturally, its spatial deviation $\tilde{\phi}$ is defined such that its spatial average equals zero $\langle \tilde{\phi} \rangle = 0$. The dialyzer matrix consists of three phases, namely blood, dialysate and membrane. Sano and Nakayama [16] introduced these averaging to individual velocities and species concentrations in dialyzer, namely, the blood, dialysate and membrane phases. Subsequently, they exploited spatial average relationships as follows:

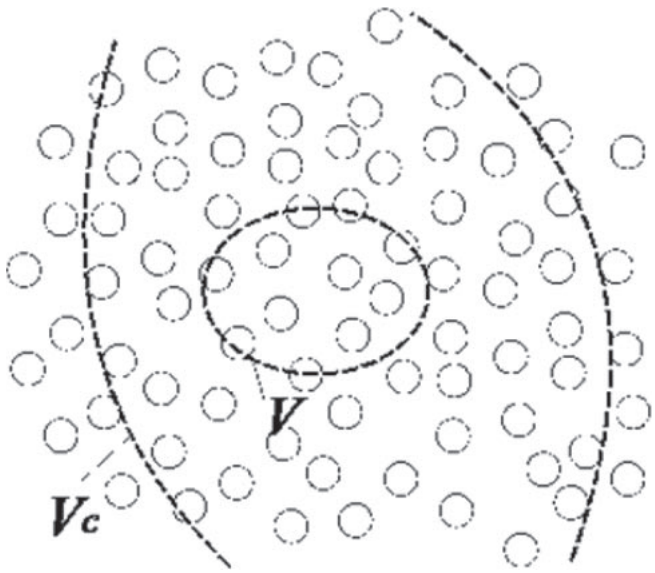

Fig. 1. Control volume in a porous medium.

$$\langle \phi_1 \phi_2 \rangle^f = \langle \phi_1 \rangle^f \langle \phi_2 \rangle^f + \langle \tilde{\phi}_1 \tilde{\phi}_2 \rangle^f \tag{5}$$

$$\left\langle \frac{\partial \phi}{\partial x_i} \right\rangle^f = \frac{1}{\varepsilon_f} \frac{\partial \varepsilon_f \langle \phi \rangle^f}{\partial x_i} + \frac{1}{V_f} \int_{A_{\text{int}}} \phi n_i dA \tag{6}$$

and

$$\left\langle \frac{\partial \phi}{\partial t} \right\rangle = \frac{\partial \langle \phi \rangle}{\partial t} \tag{7}$$

where A_{int} represents the interfaces between the fluid (blood and dialysate) and membrane matrix within the local control volume. Note n_j is the unit vector pointing outward from the fluid side to membrane matrix side.

Figure 2 schematically shows a countercurrent hollow fiber dialyzer, in which only outer fibers are shown for clarity. Several thousands of hollow fiber membranes are arranged in a dialyzer. Individual phases are separated by these hollow fiber membranes. The blood flows inside hollow fibers (lumen side) from end to end of the dialyzer. On the other hand, the dialysate is fed from the tube connected vertically near one end of the dialyzer, and then, passes through the bundles of hollow fibers. Finally, the dialysate leaves from the tube connected at opposite side of dialyzer. The microscopic governing equations, namely, the continuity, momentum and species mass transfer equations can be written as follows:

$$\frac{\partial u_j}{\partial x_j} = 0 \tag{8}$$

$$\rho \frac{\partial u_i}{\partial t} + \rho \frac{\partial u_j u_i}{\partial x_j} = -\frac{\partial p}{\partial x_i} + \mu \frac{\partial^2 u_i}{\partial x_j{}^2} \tag{9}$$

$$\frac{\partial c}{\partial t} + \frac{\partial u_j c}{\partial x_j} = D \frac{\partial^2 c}{\partial x_j{}^2} \tag{10}$$

These governing equations may be written for three individual phases. These microscopic equations are integrated over the local control volume, exploiting the foregoing spatial average relationships, as given by Eqs. (5) to (7). The set of the macroscopic governing equations for the blood phase (lumen side) may be given as follows:

$$\frac{\partial \varepsilon_b \langle u_j \rangle^b}{\partial x_j} + \int_{A_{\text{int}}} u_j n_{bj} dA = 0 \tag{11}$$

$$\rho \frac{\partial \langle u_i \rangle^b}{\partial t} + \rho \frac{\partial \langle u_j \rangle^b \langle u_i \rangle^b}{\partial x_j} = -\frac{\partial \langle p \rangle^b}{\partial x_i} + \frac{\partial}{\partial x_j} \left(\mu \frac{\partial \langle u_i \rangle^b}{\partial x_j} + \frac{\mu}{V_b} \int_{V_{b_{\text{int}}}} u_i dA - \rho \langle \tilde{u}_i \tilde{u}_j \rangle^b \right) + \frac{1}{V_b} \int_{A_{b_{\text{int}}}} \left(\mu \frac{\partial u_i}{\partial x_j} - p \delta_{ij} \right) n_{bj} dA - \frac{1}{V_b} \int_{A_{b_{\text{int}}}} \rho u_j u_i n_{bj} dA \tag{12}$$

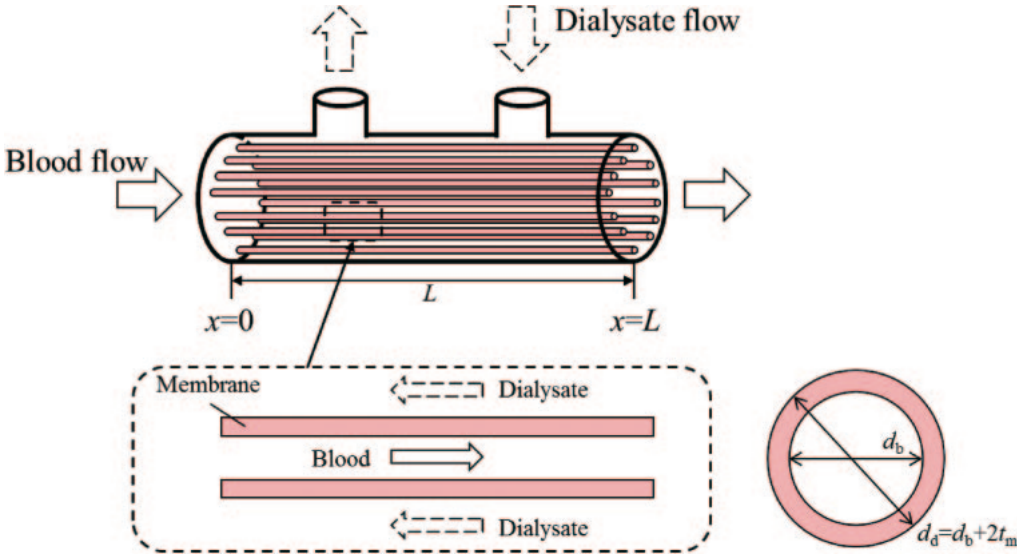

Fig. 2. Countercurrent hollow fiber dialyzer.

$$\frac{\partial \varepsilon_b \langle c\rangle^b}{\partial t} + \frac{\partial \varepsilon_b \langle u_j\rangle^b \langle c\rangle^b}{\partial x_j} = \frac{\partial}{\partial x_j}\left(\varepsilon_b D_b \frac{\partial \langle c\rangle^b}{\partial x_j} + \frac{D_b}{V}\int_{A_{b_{\text{int}}}} c n_{b_j} dA - \rho \varepsilon_b \langle \tilde{c}\tilde{u}_j\rangle^b\right) + \frac{1}{V}\int_{A_{b_{\text{int}}}} D_b \frac{\partial c}{\partial x_j} n_{bj} dA - \frac{1}{V}\int_{A_{b_{\text{int}}}} c u_j n_{bj} dA \tag{13}$$

where the superscript b indicates the blood phase. As already noted, n_{bi} is the unit vector pointing outward from the blood side to membrane side. This set of the volume averaged governing equations may be closed by means of modeling the unknown terms associated with subscales in terms of the volume averaged quantities (i.e., the dependent variables) [17, 19]. Sano and Nakayama [16] took modeling the unknown terms in the original macroscopic equations, subsequently, they introduced the macroscopic governing equations for three individual phases in dialyzer as follows:
For the blood (lumen) phase:

$$\frac{\partial \varepsilon_b \langle u_j\rangle^b}{\partial x_j} + \omega = 0 \tag{14}$$

$$\rho \frac{\partial \langle u_i\rangle^b}{\partial t} + \rho \frac{\partial \langle u_j\rangle^b \langle u_i\rangle^b}{\partial x_j} = -\frac{\partial \langle p\rangle^b}{\partial x_i} + \mu \frac{\partial^2 \langle u_i\rangle^b}{\partial {x_j}^2} - \frac{\mu}{K_{b_{ij}}} \varepsilon_b \langle u_j\rangle^b \tag{15}$$

$$\frac{\partial \varepsilon_b \langle c\rangle^b}{\partial t} + \frac{\partial \varepsilon_b \langle u_j\rangle^b \langle c\rangle^b}{\partial x_j} = \frac{\partial}{\partial x_j}\left(\varepsilon_b D_b \frac{\partial \langle c\rangle^b}{\partial x_j} + \varepsilon_b D_{b\, dis_{jk}} \frac{\partial \langle c\rangle^b}{\partial x_k}\right) - a_b h_{tb}(\langle c\rangle^b - \langle c\rangle^m) - \omega \langle c\rangle^b \tag{16}$$

For the dialysate (shell) phase:

$$\frac{\partial \varepsilon_d \langle u_j\rangle^d}{\partial x_j} - \omega = 0 \tag{17}$$

$$\rho \frac{\partial \langle u_i\rangle^d}{\partial t} + \rho \frac{\partial \langle u_j\rangle^d \langle u_i\rangle^d}{\partial x_j} = -\frac{\partial \langle p\rangle^d}{\partial x_i} + \mu \frac{\partial^2 \langle u_i\rangle^d}{\partial {x_j}^2} - \frac{\mu}{K_{d_{ij}}} \varepsilon_d \langle u_j\rangle^d \tag{18}$$

$$\frac{\partial \varepsilon_d \langle c\rangle^d}{\partial t} + \frac{\partial \varepsilon_d \langle u_j\rangle^d \langle c\rangle^d}{\partial x_j} = \frac{\partial}{\partial x_j}\left(\varepsilon_d D_d \frac{\partial \langle c\rangle^d}{\partial x_j} + \varepsilon_d D_{d\, dis_{jk}} \frac{\partial \langle c\rangle^d}{\partial x_k}\right) - a_d h_{td}(\langle c\rangle^d - \langle c\rangle^m) + \omega \langle c\rangle^m \tag{19}$$

For the membrane phase:

$$\frac{\partial \varepsilon_m \langle c\rangle^m}{\partial t} = \frac{\partial}{\partial x_j}\left(\varepsilon_m D_{m_{jk}} \frac{\partial \langle c\rangle^m}{\partial x_k}\right) + a_b h_{tb}(\langle c\rangle^b - \langle c\rangle^m) + \omega \langle c\rangle^b + a_d h_{td}(\langle c\rangle^d - \langle c\rangle^m) - \omega \langle c\rangle^m \tag{20}$$

where

$$\omega \equiv \frac{1}{V}\int_{A_{b_{\text{int}}}} u_j n_{b_j} dA = a_b L_p \left\{(\langle p\rangle^b - \langle p\rangle^d) - \sigma \frac{iR\langle T\rangle^m}{M}(\langle c\rangle^m - \langle c\rangle^d)\right\} \tag{21}$$

where the subscripts, b, d and m are assigned to indicate the blood phase, dialysate phase and membrane phase, respectively. Equations (14)–(16) are the continuity, momentum and mass balance equations for the blood phase, while Eqs. (17)–(19) describe for the dialysate phase, respectively. As defined in Eq. (21), ω is the ultrafiltration volume rate per unit volume, which penetrates through the membrane due to the pressure difference of both static pressure and osmotic pressure between blood and dialysate phases. The osmotic pressure is given by $(iR\langle T\rangle^m/M)(\langle c\rangle^m - \langle c\rangle^d)$, where i, R (= 8341 J/kg kmol K), M and $\langle T\rangle^m$ are the number of ions for ionized solutes (i.e., Vant Hoff factor), ideal gas constant, molecular weight of solute and temperature, respectively. However, in a hemodialysis, it is a common practice to control the osmotic pressure between the blood and dialysate (around 300 mOsm/l), such that the osmotic pressure can be negligible. In this model, the membrane is characterized in terms of three parameters, namely, the hydraulic permeability L_p, the solute permeability through the membrane h_m and the reflection coefficient σ. The reflection coefficient σ can be negligible when the size of molecule penetrating through the membrane is much smaller than the size of pore existing on the membrane.

In this study, as carrying out three dimensional numerical calculations based on Eqs. (14)–(21), the permeability and the dispersion tensors for both lumen and shell sides are given by reference to Sano *et al.* [24] as follows:
For the lumen side:

$$\frac{1}{K_{b_{ij}}} = \begin{bmatrix} \frac{1}{K_{b_{xx}}} & 0 & 0 \\ 0 & \frac{1}{K_{b_{yy}}} & 0 \\ 0 & 0 & \frac{1}{K_{b_{zz}}} \end{bmatrix} \tag{22}$$

$$K_{b_{xx}} = \frac{\varepsilon_b {d_b}^2}{32} \gg K_{b_{yy}} = K_{b_{zz}} = 0 \tag{23}$$

$$D_{b\,dis_{xx}} = \frac{D_b}{192}\left(\frac{\langle u\rangle^b d_b}{D_b}\right)^2 \gg D_{b\,dis_{yy}} = D_{b\,dis_{zz}} = 0 \tag{24}$$

For the shell side:

$$K_{d_{xx}} = \frac{\varepsilon_d}{32}\left(\frac{\varepsilon_d {d_b}^2}{\varepsilon_b d_d}\right)^2 \tag{25}$$

$$K_{d_{yy}} = K_{d_{zz}} = \frac{{\varepsilon_d}^3 {d_d}^2}{120(1-\varepsilon_d)} \tag{26}$$

$$D_{d\,dis_{xx}} = \frac{D_d}{192}\left(\frac{\langle u\rangle^d}{D_d}\left(\frac{\varepsilon_d {d_b}^2}{\varepsilon_b d_d}\right)\right)^2 \gg D_{d\,dis_{yy}} = D_{d\,dis_{zz}} \cong D_{d\,dis_{xx}}/20 \tag{27}$$

where the axial permeability component K_{bxx} and dispersion component D_{bxx} of the lumen side was estimated by assuming laminar fully-developed flow in a tube, while the transverse components $K_{byy} = K_{bzz}$, $D_{byy} = D_{bzz}$ may virtually be set to zero since the blood flows axially inside hollow fibers. On the other hand, the axial permeability component and dispersion component of the shell side may be evaluated by using the hydraulic diameter concept, while the transverse components are proposed by many reports [18, 25, 26] associated with the transport phenomena in porous media.

The effective mass transfer coefficients for lumen and shell sides are defined as follows:
For the lumen side:

$$\frac{1}{h_{tb}} = \frac{1}{h_b} + \frac{d_b}{2\varepsilon_p D_m}\ln\left(\frac{\frac{d_b+d_d}{2}}{d_b}\right) = \frac{1}{h_b} + \frac{d_b}{2\varepsilon_p D_m}\ln\left(1+\frac{t_m}{d_b}\right) \cong \frac{1}{h_b} + \frac{1}{2h_m} \tag{28}$$

For the shell side:

$$\frac{1}{h_{td}} = \frac{1}{h_d} + \frac{d_d}{2\varepsilon_p D_m}\ln\left(\frac{d_d}{\frac{d_b+d_d}{2}}\right) = \frac{1}{h_d} + \frac{d_b}{2\varepsilon_p D_m}\left(1+2\frac{t_m}{d_b}\right)\ln\left(\frac{1+2\frac{t_m}{d_b}}{1+\frac{t_m}{d_b}}\right) \cong \frac{1}{h_d} + \frac{1}{2h_m} \tag{29}$$

where D_m is the solute diffusion coefficient in water. The resistance of mass transfer through membrane can be shared half and half for lumen and shell sides since the membrane thickness is very thin. Shimura [27] proposed an empirical formula to estimate an interstitial mass transport coefficient of shell side in dialyzer.

$$Sh = \frac{h_d d_h}{D_m} = 4.2{Re_d}^{0.73}{Sc_d}^{1/3}(d_h/L)^{0.5} \tag{30}$$

where d_h is the hydraulic diameter for dialysate phase, Reynolds number and Schmidt number are defined as $Re_d = \langle u\rangle^d d_h/\nu_d$ and $Sc_d = \nu_d/D_m$. Moreover, he mentioned that the resistance of mass transfer for the lumen side can be consider the constant value under the hemodialysis treatment.

3. Three-Dimensional Numerical Simulation

We shall consider a hollow fiber dialyzer FDW-10 produced by Nikkiso, as illustrated in Fig. 3, in which geometrical details of dialyzer housing are shown. On the other hand, geometrical details of the follow fiber membrane are provided by the manufacturer as follows:

$$L = 26\,\text{cm},\ N = 8500,\ d_b = 210\,\mu\text{m},\ t_m = 30\,\mu\text{m},\ A_{fiber} = 1.3\,\text{m}^2$$

where N and A_{fiber} are the number of hollow fibers and the total area of hollow fibers, respectively. The membrane thickness, the inner and outer diameters of the hollow fiber are indicated by t_m, d_b and $d_d = d_b + 2t_m$, respectively. The baffle plate is arranged at entrances of dialysate phase in FDW-10 so that dialysate uniformly penetrates through the bundle of hollow fibers. The hydraulic permeability of the membrane $L_p = 2.5 \times 10^{-10}\,\text{m/sPa}$ and the solute permeability through the membrane $h_m = 1.85 \times 10^{-5}\,\text{m/s}$ are provided by Shimura [27]. The following relations can be found for the volume fractions ε_b, ε_m ε_d, the specific area of the blood compartment a_b and that of the dialysate compartment a_d:

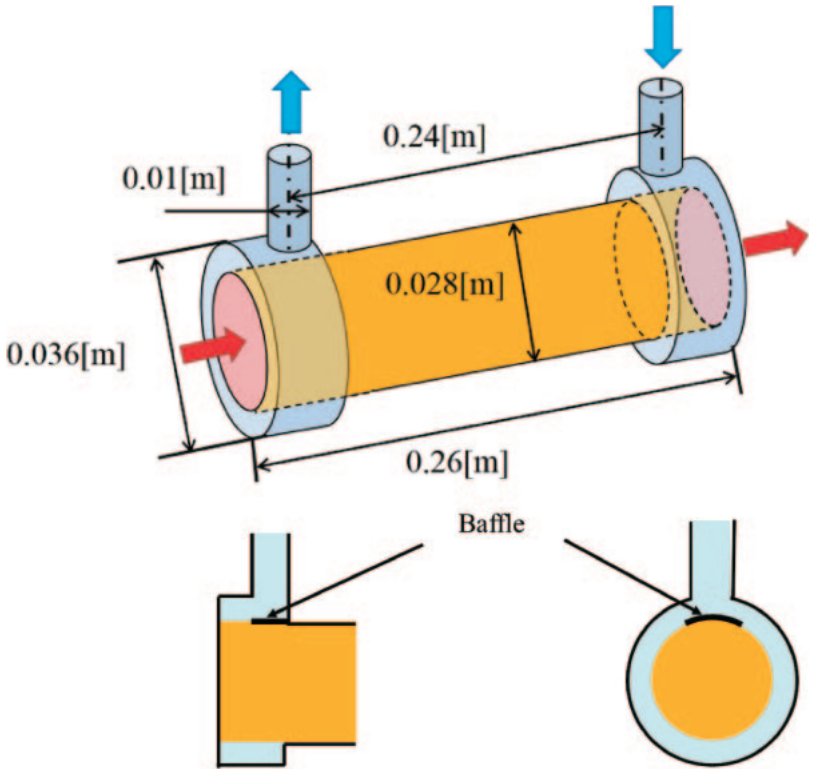

Fig. 3. Numerical model (FDW-10 produced by Nikkiso).

$$\varepsilon_b = \frac{N\frac{\pi}{4}{d_b}^2}{A} \tag{31}$$

$$\varepsilon_m = \frac{\frac{\pi}{4}((d_b + 2t_m)^2 - {d_b}^2)}{\frac{\pi}{4}{d_b}^2}\varepsilon_b = 4\frac{t_m}{d_b}\left(1 + \frac{t_m}{d_b}\right)\varepsilon_b \tag{32}$$

$$\varepsilon_d = 1 - \left(1 + 4\frac{t_m}{d_b}\left(1 + \frac{t_m}{d_b}\right)\right)\varepsilon_b \tag{33}$$

$$a_b = \frac{4\varepsilon_b}{d_b} \tag{34}$$

$$a_d = \frac{4\varepsilon_b}{d_b}\left(1 + 2\frac{t_m}{d_b}\right) \tag{35}$$

where A is the cross-sectional area of the dialyzer case.

Sano *et al.* [28] introduced the combined velocity vector to solve the continuity equations (14) and (17) containing the ultrafiltration rate.

$$\bar{u}_i \equiv \varepsilon_b \langle u_i \rangle^b + \varepsilon_d \langle u_i \rangle^d = u_{b_i} + u_{d_i} \tag{36}$$

where u_{b_i} and u_{d_i} are the Darcian velocities for blood and dialysate phases, respectively. Exploiting the combined velocity vector $\bar{u}_i$, a usual discretization procedure can be used to formulate the pressure correction equations based on SIMPLE algorithm [29]. Upon substituting Eq. (36) into the original macroscopic governing equations (14)–(16) for the dialysate phase, we obtain,

$$\frac{\partial \bar{u}_j}{\partial x_j} = 0 \tag{37}$$

$$\begin{aligned}\varepsilon_d \rho \frac{\partial \bar{u}_i}{\partial t} + \rho \frac{\partial \bar{u}_j \bar{u}_i}{\partial x_j} &= -{\varepsilon_d}^2 \frac{\partial \langle p \rangle^d}{\partial x_i} + \varepsilon_d \frac{\partial}{\partial x_j}\left(\mu \frac{\partial \bar{u}_i}{\partial x_j}\right) + \varepsilon_d \frac{\partial}{\partial x_j}\left(\mu \frac{\partial \bar{u}_j}{\partial x_i}\right) - \frac{\mu}{K_{b_{ij}}}{\varepsilon_d}^2 \bar{u}_j^d \\ &+ \frac{\partial}{\partial x_j}(\bar{u}_i u_{bj}) + \frac{\partial}{\partial x_j}(\bar{u}_j u_{b_i}) - \frac{\partial}{\partial x_j}({u_{b_i}}^2) - \varepsilon_d \frac{\partial}{\partial x_j}\left(\mu \frac{\partial u_{b_i}}{\partial x_j}\right) + \frac{\nu}{K_{d_{ij}}}{\varepsilon_d}^2 u_{b_j}\end{aligned} \tag{38}$$

$$\frac{\partial \varepsilon_d \langle c\rangle^d}{\partial t} + \frac{\partial u_{dj}\langle c\rangle^d}{\partial x_j} = \frac{\partial}{\partial x_j}\left(\varepsilon_d D_d \frac{\partial \langle c\rangle^d}{\partial x_j} + \varepsilon_d D_{d_{disjk}} \frac{\partial \langle c\rangle^d}{\partial x_k}\right) - a_d h_{td}(\langle c\rangle^d - \langle c\rangle^m) - \frac{du_b}{dx}\langle c\rangle^m \tag{39}$$

Note that the Darcian velocity of the blood phase is given by $u_{bi} = (u_{bx}, 0, 0)$ since the blood flows axially inside hollow fibers (lumen side) from end to end of dialyzers. The set of the equations for blood and membrane phases may be simplified further,

$$\frac{du_b}{dx} = -\omega = -a_b L_p(\langle p\rangle^b - \langle p\rangle^d) \tag{40}$$

$$-\frac{d\langle p\rangle^b}{dx} - \frac{\mu}{K_{bxx}} u_b = 0 \tag{41}$$

$$\frac{d}{dx} u_b \langle c\rangle^b = -a_b h_{tb}(\langle c\rangle^b - \langle c\rangle^m) - \omega\langle c\rangle^b \tag{42}$$

$$\frac{\partial \varepsilon_m \langle c\rangle^m}{\partial t} = a_b h_{tb}(\langle c\rangle^b - \langle c\rangle^m) + \omega\langle c\rangle^b + a_d h_{td}(\langle c\rangle^b - \langle c\rangle^m) - \omega\langle c\rangle^m. \tag{43}$$

The inertia and macroscopic diffusion terms in the momentum equations are neglected since the blood flows inside hollow fibers is most likely to be laminar and fully developed flow. In the mass transport equations (40) and (43), the macroscopic diffusion terms are dropped, since such effects on the solute mass transfer would be negligibly small as compared with those of the interfacial mass transfer and ultrafiltration. Substituting Eq. (40) as given above into Eqs. (41)–(42) can readily be transformed into the following ordinary differential equations.

$$\frac{1}{a_b L_p}\frac{d^2 u_b}{dx^2} - \frac{\mu}{K_{b_{xx}}} u_b = \frac{d\langle p\rangle^d}{dx} \tag{44}$$

$$\frac{d\langle c\rangle^b}{dx} = \varepsilon_b \frac{D_b}{u_b}\frac{d^2\langle c\rangle^b}{dx^2} - \frac{a_b h_{tb}}{u_b}(\langle c\rangle^b - \langle c\rangle^m) \tag{45}$$

These governing equations (37), (38), (39), (43), (44) and (45) for describing the mass transport phenomena in dialyzer can be solved numerically for given the appropriate initial and boundary conditions as referenced to the usual hemodialysis treatment. A series of numerical calculations was carried out using the finite volume method code based on SAINTS [20].

4. Results and Discussions

Cross-sectional velocity and concentration fields for blood and dialysate phases are illustrated in Figs. 4 and 5, when the dialysate and blood inlet volume flow rate are $Q_{din} = 500\,\text{ml/min}$ and $Q_{bin} = 200\,\text{ml/min}$, which commonly set in the hemodialysis. In these figures, the dialysate inlet pressure is given as boundary condition so as to achieve the total ultrafiltration rate $Q_f = Q_{bin} - Q_{bout} = Q_{dout} - Q_{din} = 20\,\text{ml/min}$. As can be seen from Fig. 4, the dialysate permeates uniformly into the hollow fiber bundle due to baffle plates and spaces surrounding the hollow fiber bundle at both inlet and outlet for the dialysate phase. The velocity of the blood phase decreases from 5.4×10^{-3} to $4.8 \times 10^{-3}\,\text{m/s}$ as it flows from left to right in a dialyzer, since the water penetrates through membranes from blood to dialysate phases as an ultrafiltration. On the other hand, Fig. 5 shows that the concentration distributions for blood and dialysate phases exist in a dialyzer. As can be seen from Fig. 5, the mass transportation of urea reduces toward the center of the bundle from outside of a dialyzer under the influence of the deviation of the dialysate flow.

Shimura [27] carried out a careful experiment to measure the total ultrafiltration rate and urea clearance under several operating conditions by using FDW-10 produced by Nikkiso. They utilized the aqueous solution of urea in place of the blood and the dialysis for an accurate measurement of urea clearance. In this study, a series of numerical simulations were carried out along his experimental conditions to examine the validity of the present numerical method. Figure 6 shows the total ultrafiltration rate of water penetrated through hollow fiber membranes when both pressures of shell and lumen sides were set the conditions presented by Shimura [27]. The total ultrafiltration rate increases linearly with the pressure difference between shell and lumen sides. The total ultrafiltration rate obtained from the present numerical simulation agree well with a set of available experimental data. Figures 7 and 8 show urea clearance $CL = (Q_{b_{in}}\bar{c}_{b_{in}} - Q_{b_{out}}\bar{c}_{b_{out}})/\bar{c}_{b_{in}}$, which is often used for the scale for the dialysis time, against the volume flow rates of shell and lumen sides, where $\bar{c}_b$ is the bulk mean solute concentration. In Fig. 7, urea clearance increases with increasing the volume flow rate for the shell side. On the other hand, the effect of increasing the volume flow rate of blood phase on urea clearance tends to less in the case of the high blood volume flow rates under the constant volume flow rate of the dialysate phase. Moreover, urea clearance increases with increasing the volume flow rate of lumen side in Fig. 8. On the other hand, the effect of increasing the dialysate volume flow rate on urea clearance also tend to less in

the case of high dialysate volume flow rates under the constant blood volume flow rate. A good agreement between the present numerical simulation and experimental data (together with the catalog provided by the manufacturer) can be seen from these figures, which substantiate the validity of the present numerical method based on the volume averaging theory.

○Velocity fields

Blood phase

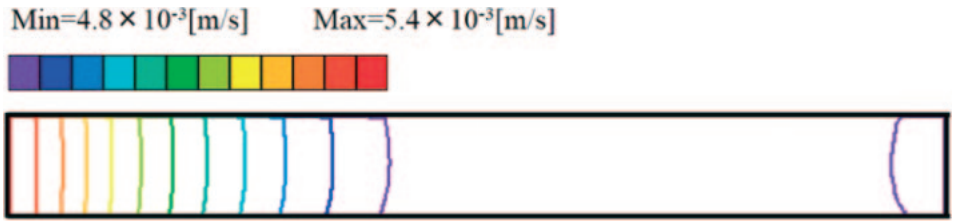

Dialysate phase

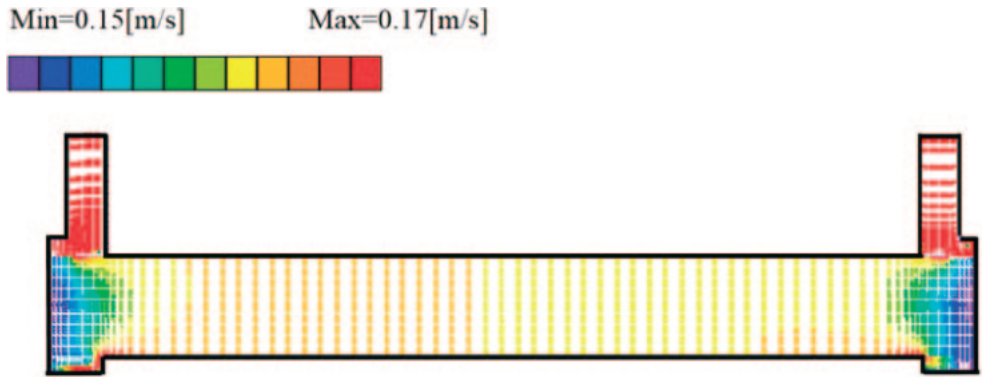

Fig. 4. Velocity fields for blood and dialysate phases.

○Concentration fields (Urea)

Blood phase

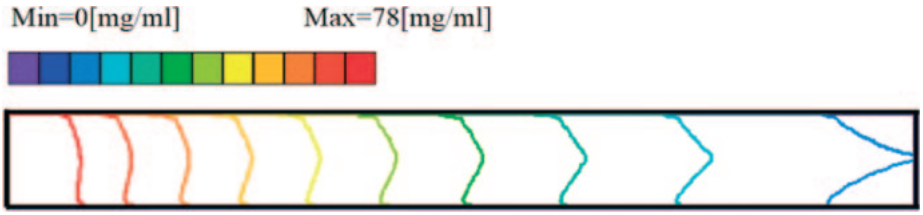

Dialysate phase

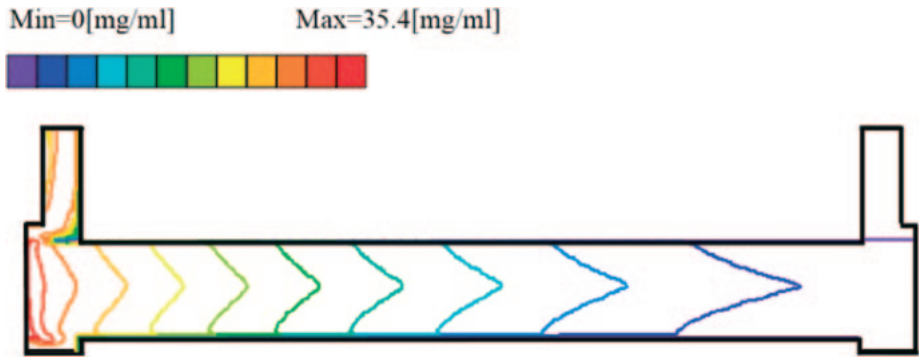

Fig. 5. Concentration fields for blood and dialysate phases.

In order to develop novel dialyzers, it is necessary to know all clearances in any case of the volume flow rates for blood and dialysate phases. Moreover, minimization of the amount of dialysate may be needed in the case you want to

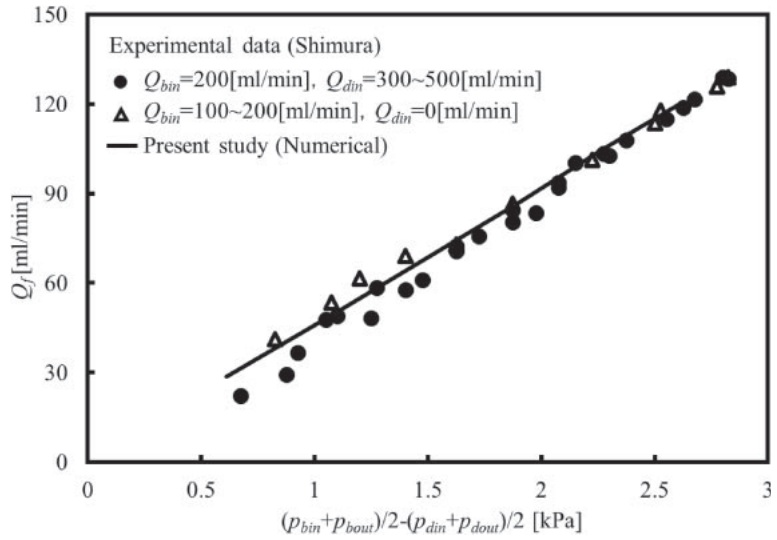

Fig. 6. Total ultrafiltration rate Q_f.
(●,△: Experiment by Shimura [27], —: Present study, L = 26 cm, N = 8500, d_b = 210 μm, tm = 30 μm, Lp = 2.5 × 10–10 m/sPa)

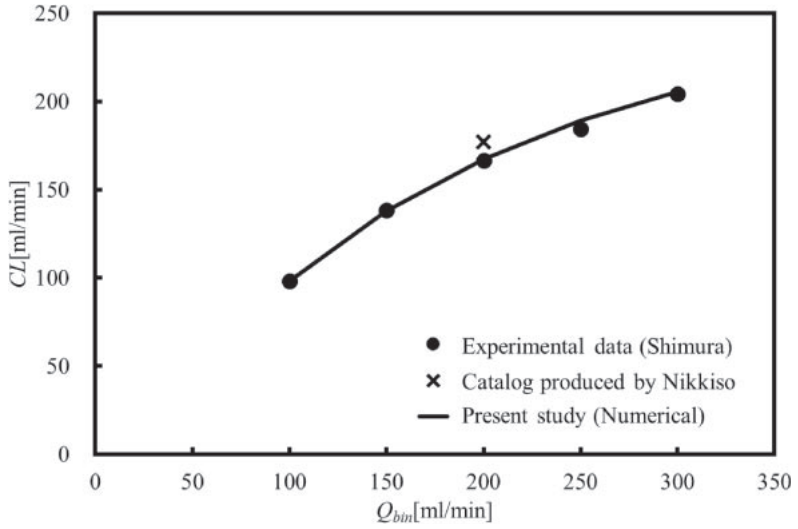

Fig. 7. Urea clearance against the volume flow rate of the lumen side.
(●: Experiment by Shimura [27], ×: Catalog, —: Present study, L = 26 cm, N = 8500, db = 210 μm, tm = 30 μm, Lp = 2.5 × 10^{-10} m/sPa, $h_m = 1.85 \times 10^{-5}$ m/s, $h_b = 1.26 \times 10^{-4}$ m/s, $D = 1.29 \times 10^{-9}$ m^2/s, Q_{bin} = 100–300 ml/min, Q_{din} = 500 [ml/min], Q_f = 0 [ml/min])

reuse the dialysate in an artificial kidney. Figure 9 shows urea clearance against the dialysate volume flow rate under the several blood volume flow rates and total ultrafiltration rates. Now, we shall introduce the removal efficiency $\varsigma = CL/\bar{Q}_{b_{in}}$, which is the ratio of the mass flow rate of urea removed from the blood phase within a dialyzer to that at the blood phase inlet, as illustrated in Fig. 10. It is found that an appropriate dialysate volume flow rate exists against each blood volume flow rate in the hemodialysis treatment. Thus, in reference to Fig. 10, it is possible that both blood and dialysate volume flow rates can be reduced in the home hemodialysis carried out for a long period. Figure 11 shows the amount of dialysate to achieve each removal efficiency. If we select a high removal efficiency, the much amount of dialysate is required as compared with a low removal efficiency. Now, we also introduce new index $(\bar{c}_{d_{out}} - \bar{c}_{d_{in}})/(\bar{c}_{b_{in}} - \bar{c}_{d_{in}})$, which is the value indicated an effective mass transfer capability of the outlet dialysate. $(\bar{c}_{d_{out}} - \bar{c}_{d_{in}})/(\bar{c}_{b_{in}} - \bar{c}_{d_{in}}) = 0$ means the inlet dialysate concentration, thus the dialysate with low concentration flows out from the dialyzer when this value is small. Figure 12 reveals that the dialysate not sufficiently exchanged waste products flows out from the dialyzer in the case of a high removing efficiency. The present numerical simulation reveals the complex transport phenomena associated with blood phase, dialysate phase and membrane phase under the several operating conditions in the hemodialysis treatment. Figures 9–12 presented in this study must be important indices in order to develop the novel dialysis treatment.

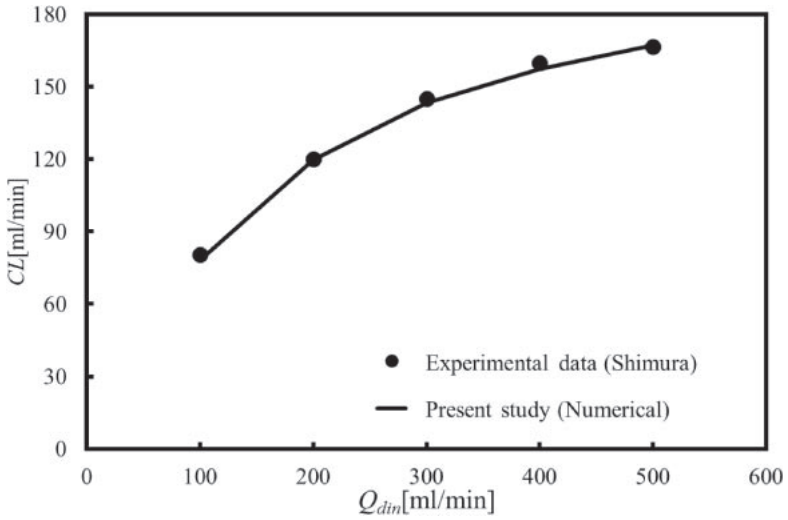

Fig. 8. Urea clearance against the volume flow rate of the shell side.
(●: Experiment by Shimura [27], —: Present study, L = 26 cm, N = 8500, db = 210 μm, tm = 30 μm, Lp = 2.5×10^{-10} m/sPa, $h_m = 1.85 \times 10^{-5}$ m/s, $h_b = 1.26 \times 10^{-4}$ m/s, D = 1.29×10^{-9} m^2/s, Q_{bin} = 200 ml/min, Q_{din} = 100–500 [ml/min], Q_f = 0 [ml/min])

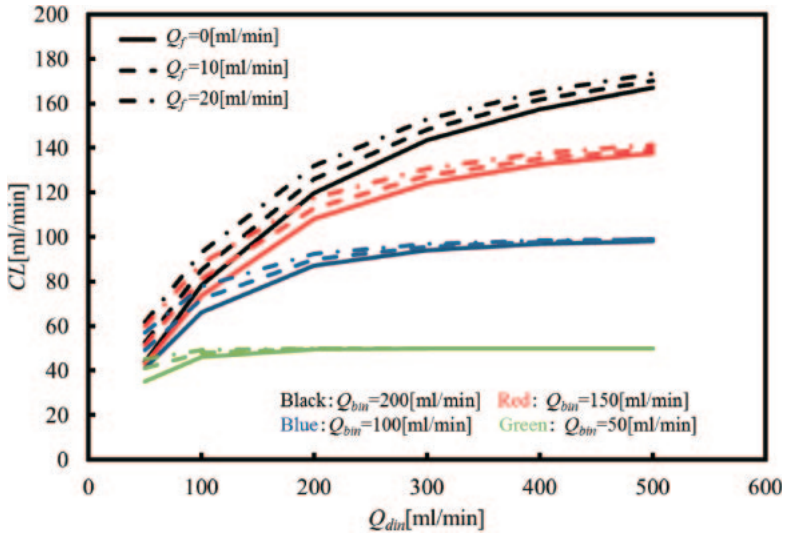

Fig. 9. Urea clearance under the several operating conditions.
(L = 26 cm, N = 8500, db = 210 μm, tm = 30 μm, Lp = 2.5×10^{-10} m/sPa, $h_m = 1.85 \times 10^{-5}$ m/s, $h_b = 1.26 \times 10^{-4}$ m/s, D = 1.29×10^{-9} m^2/s, Q_{bin} = 50–200 ml/min, Q_{din} = 50–500 [ml/min], Q_f = 0–20 [ml/min])

5. Conclusions

The effect of operating conditions on urea clearance for the hemodialysis treatment was investigated by three-dimensional numerical computations based on the volume averaging theory. A general set of macroscopic governing equations for describing the mass transport phenomena in dialyzers were derived for the three individual phases, namely, the blood (lumen) phase, the dialysate (shell) phase and the membrane phase. Numerical computations revealed cross-sectional velocity fields and concentration fields for blood and dialysate phases within a dialyzer FDW-10 produced by Nikkiso. The validity of the present numerical method was educated comparing between an available set of experimental data (together with the catalog data provided by the manufacturer) and the present numerical results. A series of numerical simulations revealed urea clearance against the dialysate volume flow rate and the blood volume flow rate under the total ultrafiltration rates. Subsequently, new indices for the hemodialysis treatment were introduced in order to estimate the appropriate volume flow rate for blood and dialysate phases. The present study clearly indicates that the present numerical method is quite useful for determining the best clinical protocol of the hemodialysis treatment and developing new dialysis systems such as home hemodialysis, nocturnal dialysis and even wearable artificial kidney.

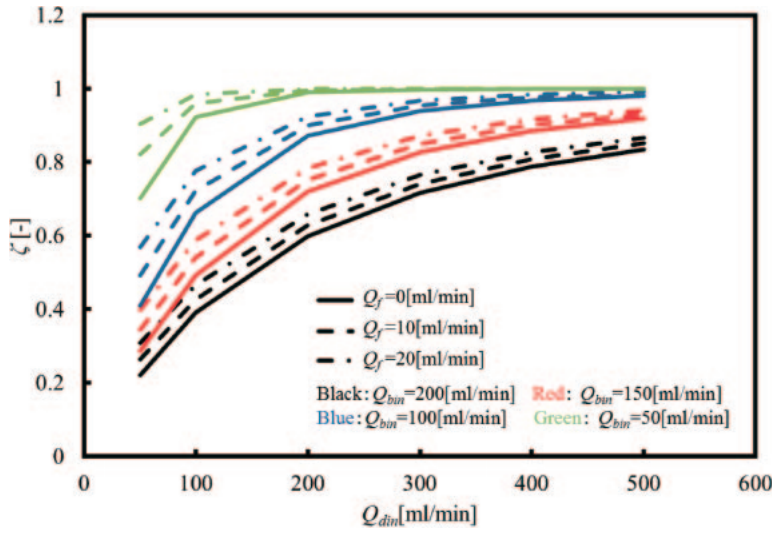

Fig. 10. Removal efficiency under the several operating conditions.
(L = 26 cm, N = 8500, db = 210 μm, tm = 30 μm, Lp = 2.5×10^{-10} m/sPa, $h_m = 1.85 \times 10^{-5}$ m/s, $h_b = 1.26 \times 10^{-4}$ m/s, D = 1.29×10^{-9} m^2/s, Q_{bin} = 50–200 ml/min, Q_{din} = 50–500 [ml/min], Q_f = 0–20 [ml/min])

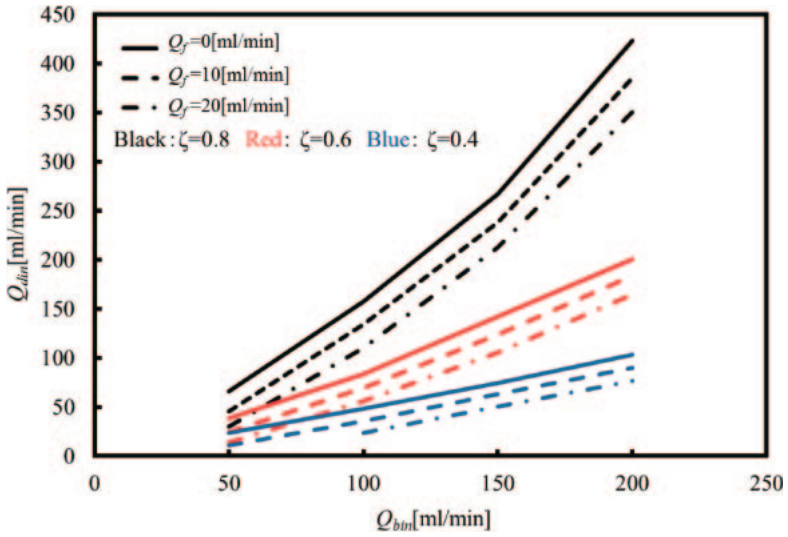

Fig. 11. The amount of dialysate in order to achieve each removal efficiency.
(L = 26 cm, N = 8500, db = 210 μm, tm = 30 μm, Lp = 2.5×10^{-10} m/sPa, $h_m = 1.85 \times 10^{-5}$ m/s, $h_b = 1.26 \times 10^{-4}$ m/s, D = 1.29×10^{-9} m^2/s, Q_{bin} = 50–200 ml/min, Q_{din} = 50–500 [ml/min], Q_f = 0–20 [ml/min])

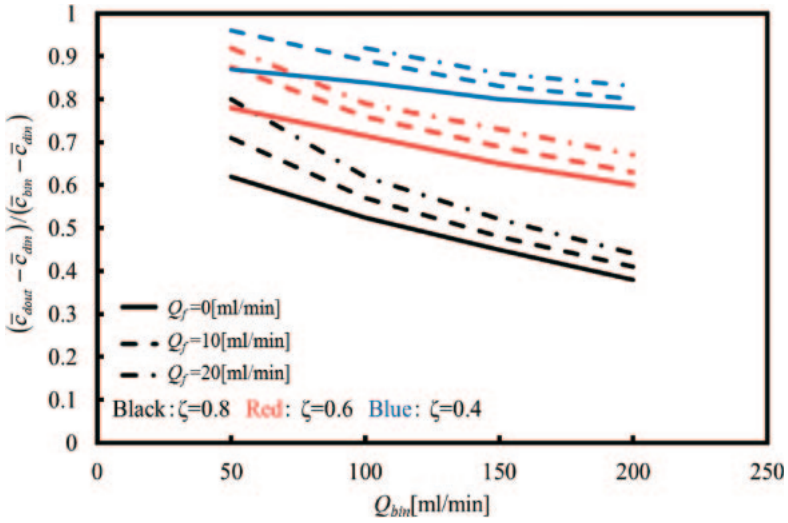

Fig. 12. $(\bar{c}_{d_{out}} - \bar{c}_{d_{in}})/(\bar{c}_{b_{in}} - \bar{c}_{d_{in}})$ under the several operating conditions.
(L = 26 cm, N = 8500, db = 210 μm, tm = 30 μm, Lp = 2.5×10^{-10} m/sPa, $h_m = 1.85 \times 10^{-5}$ m/s, $h_b = 1.26 \times 10^{-4}$ m/s, D = 1.29×10^{-9} m^2/s, Q_{bin} = 50–200 ml/min, Q_{din} = 50–500 [ml/min], Q_f = 0–20 [ml/min])

6. Nomenclature

A : cross-sectional area of the dialyzer case [m^2]
A_{fiber} : total area of hollow fibers [m^2]
$Aint$: interface area between the fluid and membrane phases [m^2]
$a_{b,d}$: specific surface area [1/m]
c : solute concentration [kg/m^3]
CL : clearance [m^3/s]
$d_{b,d}$: inner and outer diameters of the hollow fiber [m]
d_h : hydraulic diameter [m]
D : solute diffusion coefficient [m^2/s]
$D_{dis_{jk}}$: dispersion tensor [m^2/s]
h : interstitial mass transfer coefficient [m/s]
h_m : solute permeability [m/s]
i : Vant Hoff factor
K : permeability [m^2]
L : effective length of the dialyzer case [m]
L_p : hydraulic permeability of membrane [m/s Pa]
M : molecular weight of the solute [–]
n_i : unit vector pointing outward from the fluid side to membrane side [–]
N : number of hollow fibers [–]
P : pressure [Pa]
Q : volume flow rate [m^3/s]
Q_f : total ultrafiltration rate [m^3/s]
R : universal gas constant [J/kg kmol K]
Re : Reynolds number [–]
Sc : Schmidt number [–]
Sh : Sherwood number [–]
t_m : membrane thickness [m]
T : temperature [K]
$\bar{u}_i$: combined velocity vector [m/s]
u_i : velocity vector [m/s]
u_{d,b_j} : Darcian velocity vector [m/s]
V : representative elementary volume [m^3]
V_b : volume space which the fluid occupies [m^3]
x, y, z : Cartesian coordinates [m]

Greek symbols
ε : volume fraction [–]
μ : viscosity [Pa s]
ρ : density [kg/m^3]
σ : reflection coefficient [–]
ς : removal efficiency [–]
ω : perfusion rate [1/s]

Special symbols
$\tilde{\phi}$: deviation from intrinsic average
$\langle\phi\rangle$: volume average
$\langle\phi\rangle^{b,d,m}$: intrinsic average

Subscripts and superscripts
in : inlet
b : blood
d : dialysate
dis : dispersion
f : fluid
m : membrane
out : outlet

REFERENCES

[1] Davenport, A., Gura, V., Ronco, C., Beizai, M., Ezon, C., and Rambod, E., "Warable haemodialysis device for patients with end-stage renal failure: A pilot study," *The Lancet*, **370-9604**: 2005–2010 (2007).

[2] Gura, V., Macy, A. S., Beizai, M., Ezon, C., and Golper, T. A., "Technical breakthroughs in the wearable artificial kidney (WAK)," *Clinical Journal of the American Society of Nephrology*, **4–9**: 1441–1448 (2009).

[3] Kedem, O., and Katchalsky, A., "Thermodynamics analysis of the permeability of biological membranes to non-electrolytes," *Biochim. Biophys. Acta*, **27**: 229–246 (1958).

[4] Lu, J.-F., and Lu, W.-Q., "A numerical simulation for mass transfer through the porous membrane of parallel straight channels," *Int. J. Heat Mass Transfer*, **53**: 2404–2413 (2010).

[5] Tu, J.-W., Ho, C.-D., and Chuang, C.-J., "Effect of ultrafiltration on the mass-transfer efficiency improvement in a parallel-plate countercurrent dialysis system," *Desalination*, **242**: 70–83 (2009).

[6] Tu, J.-W., Ho, C.-D., and Yeh, H.-M., "The analytical and experimental studies of the parallel-plate concurrent dialysis system coupled with ultrafiltration," *J. Membrane Science*, **281**: 676–684 (2006).

[7] Yeh, H. M., "Numerical analysis of mass transfer in double-pass parallel-pale dialyzers with external recycle," *Computers and Chemical Engineering*, **33**: 815–821 (2009).

[8] Legallais, C., Catapano, G., Von Harten, B., and Baurmeister, U., "A theoretical model to predict the vitro performance of hemodiafilters," *J. Membrane Science*, **168**: 3–15 (2000).

[9] Palaty, Z., Zakova, A., and Petrik, P., "A simple treatment of mass transfer data in continous dialyzer," *J. Membrane Science*, **45**: 806–811 (2006).

[10] Galach, M., Ciechanowska, A., Sabalinska, S., Waniewski, J., Wojcicki, J., and Werynski, A., "Impact of convective transport on dialyzer clearance," *J. Artificial Organs*, **6**: 42–48 (2003).

[11] Yeh, H. M., Cheng, T.-W., and Wu, H.-H., "Membrane unltrafiltration in hollow-fiber module with the consideration of pressure declination along the fibers," *Separation and Purification Technology*, **13**: 171–180 (1998).

[12] Sigdell, J. E., "Calculation of combined diffusive and convective mass transfer," *J. Artificial Organs*, **5**: 361–372 (1982).

[13] Waniewski, J., "Mathematical modelling of fluid and solute transport in hemodialysis and peritoneal dialysis," *J. Membrane Science,* **274**: 24–37 (2006).

[14] Shirazian, S., Moghadassi, A., and Moradi, S., "Numerical simulation of mass transfer in gas-liquid hollow fiber membrane contactors for laminar flow conditions," *Simulation Modelling Practice and Theory*, **17**: 708–718 (2009).

[15] Wang, Y., Brannock, M., Cox, S., and Leslie, G., "CFD simulations of membrane filtration zone in a submerged hollow fiber membrane bioreactor using a porous media approach," *J. Membrane Science*, **363**: 57–66 (2010).

[16] Kumar, V., and Upadhyay, S. N., "Computer simulation of membrane processes: Ultrafiltration and dialysis units," *Computers and Chemical Engineering*, **23**: 1713–1724 (2000).

[17] Sano, Y., and Nakayama, A., "A porous media approach for analyzing a countercurrent dialyzer system," *ASME Trans. J. Heattransfer*, **134**: 072602-11 (2012).

[18] Cheng, P., Heat Transfer in Geothermal Systems, Advances in Heat Transfer, **14**: 1–105, Academic Press, New York (1978).

[19] Quintard, M., and Whitaker, S., "One and two equation models for transient diffusion processes in two-phase systems," *Advances in Heat Transfer*, **23**: 369–465 (1993).

[20] Nakayama, A., PC-aided Numerical Heat Transfer and Convective Flow, CRC Press, Boca Raton (1995).

[21] Vafai, K., and Tien, C. L., "Boundary and inertia effects on flow and heat transfer in porous media," *Int. J. Heat Mass Transfer*, **24**: 195–203 (1981).

[22] Nakayama, A., and Kuwahara, F., "A general bioheat transfer model based on the theory of porous media," *Int. J. Heat Mass Transfer*, **51**: 3190–3199 (2008).

[23] Yang, C., and Nakayama, A., "A synthesis of tortuosity and dispersion in effective thermal conductivity," *Int. J. of Heat and Mass Transfer*, **53**, Issues 15–16: 3222–3230 (2010).

[24] Sano, Y., Horibe, A., Haruki, N., Nagase, K., and Nakayama, A., "Numerical approach for optimal design of a hollow fiber dialyzer system," *Open Journal of Heat, Mass and Momentum Transfer*, **2**: 58–69 (2014).

[25] Nakayama, A., Kuwahara, F., and Kodama, H., "An equation for thermal dispersion flux transport and its mathematical modelling for heat and fluid flow in a porous medium," *J. of Fluid Mechanics*, **563**: 81–96 (2006).

[26] Kuwahara, F., Nakayama, A., and Koyama, H., "A numerical study of thermal dispersion in porous media," *J. Heat Transfer*, **118**: 756–761 (1996).

[27] Shimura, T., "Flow and Mass Transport Characteristics within a Dialyzer," M.S. Thesis, Shizuoka University, March (2015).

[28] Sano, Y., Nishimura, T., and Nagase, K., "A porous media approach for hollow fiber transport phenomena," *Open Journal of Heat, Mass and Momentum Transfer*, **2**, 11–27 (2014).

[29] Patankar, S. V., Numerical Heat Transfer and Fluid Flow, Washington, D.C., Hemisphere (1980).